Changing the dress to a MOF through perfluorination and transmetallation. Structural and Gas-Sorption Effects

Davide Balestri[†], Irene Bassanetti[‡], Stefano Canossa[†, ⊥], Cristina Gazzurelli[†], Alessia Bacchi[†], Silvia Bracco[‡], Angiolina Comotti[‡], Paolo Pelagatti[†,#]*

[†] Department of Chemical Sciences, Life Sciences and Environmental Sustainability, University of Parma, Viale delle Scienze, 17A, 43124, Parma, Italy.

[‡] Department of Materials Science, University of Milano-Bicocca, via Roberto Cozzi, 55, 20125 Milano, Italy.

[#] Interuniversity Consortium Chemical Reactivity and Catalysis (CIRCC), Via Celso Ulpiani 27, 70126, Bari, Italy

ABSTRACT Two novel pillared Zn(II)-based Metal-Organic Frameworks were *de-novo* synthesized exploiting *N,N'-(1,1'-biphenyl)-4,4'-diylbis-4-pyridinecarboxamide* (bpba) and its fluorinated analogous *N,N'-(perfluoro-1,1'-biphenyl-4,4'-diyl)diisonicotinamide* (F-bpba) as suitable pillar linkers and 2,6-naphthalene dicarboxylic acid as carboxylic ligand. The resulting heteroleptic MOFs, namely **PUM210**, $[Zn_4(bpba)_{1.5}\cdot(ndc)_4\cdot(H_2O)]_n$ and **PUM210F**, $[Zn_3(F-bpba)_1\cdot(ndc)_3\cdot(DMF)]_n$, feature an uncommon truncation of the Zn(II) paddle-wheel nodes along

the pillaring direction. **PUM210** and **PUM210F** exhibit a polycatenated architecture, resulting in microporous channels decorated by amide moieties. The activated forms show a permanent porosity and a selective adsorption of CO_2 over N_2. Moreover, the partially transmetallated **Cu-PUM210** and **Cu-PUM210F** were obtained by convenient transmetallation protocol and their adsorption propriety towards CO_2 were subsequently investigated.

INTRODUCTION

Among porous materials, Metal-Organic Frameworks (MOFs) are well-known for the high versatility of their structural design and tailoring.[1,2] This comes from the possibility of selecting the most appropriate ligands and metal nodes to reach the desired architecture, which can be further tuned by post-synthetic modifications (PSM). Among the most effective PSM protocols, transmetallation,[3] i.e. the replacement of framework metal ions, is of particular interest, because it can have profound effects not only on the final crystalline structure, in some occasions leading to the isolation of solid phases not obtainable under conventional synthetic protocols,[4–6] but even on framework stability,[7] porosity and then uptake properties.[8] In particular, the selectivity towards CO_2 trapping is of paramount relevance, owing to the dramatic environmental issues linked to this greenhouse gas.[9–11] Significant enhancements of both carbon dioxide uptake and selectivity have been reached exploiting the quadrupolar moment of CO_2.[12,13] Hence, a wide applied protocol regards the introduction of polar groups, such as amine[14–16] or amide,[17,18] in the MOF framework to strengthen the interactions between CO_2 molecules and the MOF internal walls. In particular, amide groups can interact with carbon dioxide through N-H…O=CO hydrogen-bonds or act as Lewis base through N…CO contacts.[19–21] Another successful strategy which can be exploited for the preparation of good sorbents is based on perfluorination or partial

fluorination of organic linkers. Although a favorable effect is not easily predictable *a priori*, in some cases significant enhancements of carbon dioxide trapping have been observed.[22–25]

Starting from these considerations, we decided to employ the two amide-containing ligands *N,N'-(1,1'-biphenyl)-4,4'-diylbis-4-pyridinecarboxamide* (**bpba**) and its fluorinated analogous *N,N'-(perfluoro-1,1'-biphenyl-4,4'-diyl)diisonicotinamide* (**F-bpba**) for the self-assembly of novel pillared MOFs[26] (Scheme 1). The two ligands have the same length and then are expected, once combined with the same di-carboxylate ligand and the same SBU, to lead to structurally very similar pillared MOFs. However, the perfluorinated biphenyl core of **F-bpba** allows to evaluate the effect of perfluorination on the carbon dioxide uptake. To the best of our knowledge, **bpba** has rarely been used for the construction of metal-containing assemblies,[27] while its use in MOF synthesis has been recently reported by us.[28] **F-bpba** is a new bis-pyridine ligand never reported in literature.

The two ligands were used to assemble two new heteroleptic pillared MOFs, $[Zn_4(bpba)_{1.5}\cdot(ndc)_4\cdot(H_2O)]_n$ (**PUM210**) and $[Zn_3(F\text{-}bpba)_1\cdot(ndc)_3\cdot(DMF)]_n$ (**PUM210F**) (PUM stands for Parma University Materials), which were structurally characterized by single crystal X-ray analysis. Moreover, the corresponding partially transmetallated Cu-MOFs were obtained through a mild transmetallation protocol yielding to the heterometallic Zn^{2+}-Cu^{2+} materials **Cu-PUM210** and **Cu-PUM210F**. In this work the structural differences arising from perfluorination and transmetallation will then be discussed, together with the sorption properties of the isolated crystalline materials towards CO_2, N_2 and CH_4, with particular regard to the CO_2 selective adsorption.
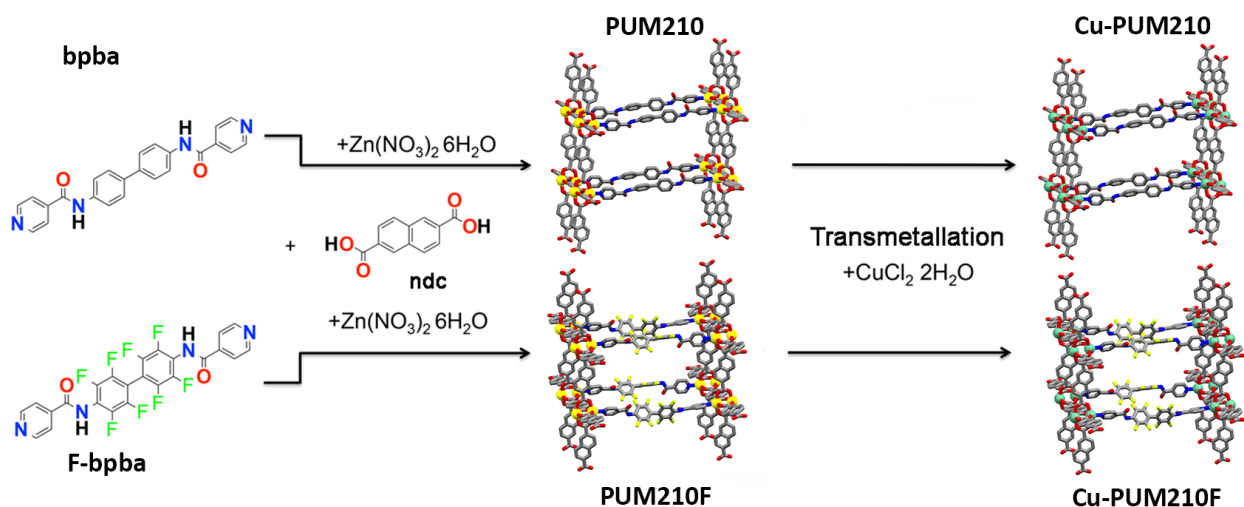
Scheme1. Schematic representation of the synthesis of the MOFs shown in this work

EXPERIMENTAL SECTION

Materials and Methods: The ligand *N,N'-(1,1'-biphenyl)-4,4'-diylbis-4-pyridinecarboxamide* (**bpba**) was synthesized according to the previously published Pd-catalyzed cross-coupling protocol optimized in our laboratory.[29] *N,N'-(perfluoro-1,1'-biphenyl-4,4'-diyl)diisonicotinamide* (**F-bpba**) was synthesized according to the procedure described below. 2,6-naphthalendicarboxylic acid (ndc) and all other reagents and solvents are commercially available and were used as received.

Physical and Chemical Measurements. The details of the apparatus used for the spectroscopic and thermal characterization are given in the Supporting Information.

Single Crystal X-ray Crystallography (SC-XRD): Crystal measurements were performed at Elettra Syncrotron (Trieste, Italy) on beamline XRD1 at 100K under cold nitrogen flux.[30] The source used for the analysis was a NdBFe Multipole Wiggler (Hybrid linear), 4.27 KeV with a power of 8.6 kW, a source size FWHM of 2.0 x 0.37 mm (0.7 x 0.2 mm FWHM beam size at sample) and photon flux 1012-1013 ph/sec. MOFs crystals were taken from the mother liquor or washing DMF and mounted with cryoloops (0.05-0.3 mm), prior a flash freezing at 100 K.

Diffraction data were indexed, integrated, and scaled using CrysAlis software. Structures were solved by direct methods using SHELXS[31] and refined by full-matrix least-squares on all F2 using SHELXL implemented in Olex2.[32] For all the structures, anisotropic displacement parameters were refined except for hydrogen atoms. Unstructured residual electron density found inside cavities was accounted for by the Mask procedure in Olex. Table 1 reports the results of crystal structures determination. Crystallographic data for **PUM210**, **PUM210F**, and **Cu-PUM210F** have been deposited with the Cambridge Crystallographic Data Centre (1849457-1849459) .

Table 1. Crystal data and structural refinement.

	PUM210	PUM210F	Cu-PUM210F
Empirical formula	$C_{186}H_{148}N_{18}O_{46}Zn_8$	$C_{63}H_{35}F_8N_5O_{15}Zn_3$	$C_{72}H_{56}Cu_3F_8N_8O_{18}$
Formula weight	3894.18	1450.07	1663.86
Temperature/K	100.0	100.0	100.0
Crystal system	monoclinic	monoclinic	monoclinic
Space group	C2/c	P21/c	P21/c
a/Å	18.9998(6)	31.7870(4)	31.6781(17)
b/Å	18.0175(5)	17.3848(2)	17.4634(4)
c/Å	62.1271(16)	19.5421(3)	19.4796(7)
α/°	90	90	90
β/°	90.557(2)	97.3440(10)	97.172(3)
γ/°	90	90	90
Volume/Å^3	21266.9(10)	10710.6(2)	10691.9(7)
Z	4	4	4
ρcalcg/cm3	1.216	0.899	1.034
F(000)	7992.0	2920.0	3388.0
2Θ range for data collection/°	3.32 to 51.888	3.1 to 57.298	3.446 to 51.888
Index ranges	-23 ≤ h ≤ 23, -20 ≤ k ≤ 20, -74 ≤ l ≤ 76	-43 ≤ h ≤ 43, -23 ≤ k ≤ 23, -26 ≤ l ≤ 26	-37 ≤ h ≤ 39, -21 ≤ k ≤ 21, -23 ≤ l ≤ 23
Reflections collected	57163	175080	44236
Independent reflections	21249 [Rint = 0.0748, Rsigma = 0.0589]	28514 [Rint = 0.0505, Rsigma = 0.0240]	20826 [Rint = 0.0504, Rsigma = 0.0579]
Data/restraints/parameters	21249/636/1084	28514/517/1098	20826/301/1431
Goodness-of-fit on F2	2.725	1.062	1.429
Final R indexes [I>=2σ (I)]	R1 = 0.2301, wR2 = 0.5843	R1 = 0.0638, wR2 = 0.2089	R1 = 0.1045, wR2 = 0.3472
Final R indexes [all data]	R1 = 0.2437, wR2 = 0.5923	R1 = 0.0702, wR2 = 0.2165	R1 = 0.1188, wR2 = 0.3615

Largest diff. peak/hole / e Å^{-3} 4.34/-3.98   1.25/-0.83   1.43/-1.61

*Synthesis of **F-bpba***. In a 250 mL two neck round bottomed flask, octafluorobenzidine (0.50 g, 1.52 mmol), triethylamine (1.0 mL, 7.30 mmol, 4.8 equivalents) and isonicotinoyl chloride hydrochloride (0.65 g, 3.65 mmol, 2.4 equivalents) were added to dry toluene (30 mL). The resulting reaction mixture was heated at reflux for 5 days. Then, water (30 mL) was added and the crude was isolated by vacuum filtration. The resulting off-white solid was washed with water (3x10 mL) and ethanol and dried to provide **F-bpba** (0.61 g, 1.12 mmol, y = 74%). ^{1}H-NMR (400 MHz, DMSO-d^6, 25°C) δ: 11.19 (s, 2H, NH), 8.87 (d, J = 5.6 Hz, 4H, CH$_{pyr}$), 7.94 (d, J = 5.6 Hz, 4H, CH$_{pyr}$) ppm; ^{19}F{^{1}H}-NMR (377 MHz, DMSO-d^6, 25°C) δ: -139.12 (m), -143.43 (m) ppm; ^{13}C{^{1}H}-NMR (100 MHz, DMSO-d^6, 25°C): 164.6 (C=O), 151.1 (CH), 144.2 (dd, $^1J_{CF}$= 251.0 Hz, $^2J_{CF}$= 14.0 Hz, CF), 142.5 (dd, $^1J_{CF}$= 251.0 Hz, $^2J_{CF}$= 14.0 Hz, CF), 139.8 (C-C=O), 112.3 (CH), 119.8 (m, C-N ipso), 104.5 (m, C-CF ipso) ppm; IR (ATR, cm^{-1}): 3235, 1687, 1516, 1496, 1468, 1413, 1299, 987, 915, 845, 759, 737, 728, 711, 670, 654, 618; MS (ESI +) : m/z 539.1 [M +H]$^+$.

*Synthesis of **PUM210***: In a 70 mL pyrex glass tube, **bpba** (0.2 mmol, 80 mg), 2,6-naphthalendicarboxylic acid (0.4 mmol, 86 mg) and Zn(NO$_3$)$_2$·6H$_2$O (0.4 mmol, 120 mg) were added to DMF (41 mL). The resulting mixture was sonicated, then heated under autogenous pressure at 80°C. After 5 days the reaction vessel was slowly cooled to room temperature. The resulting small yellow crystals were washed with DMF (2 x 10 mL).

*Synthesis of **PUM210F***: In a 20 mL pyrex glass tube, **F-bpba** (0.1 mmol, 54 mg), 2,6-naphthalendicarboxylic acid (0.2 mmol, 40 mg) and Zn(NO$_3$)$_2$·6H$_2$O (0.2 mmol, 60 mg) were added to DMF (10 mL). The resulting mixture was sonicated, then heated under autogenous

pressure at 80°C. After 5 days, the reaction vessel was slowly cooled to room temperature. The resulting colourless small crystals were washed with DMF (2 x 10 mL).

Transmetallation reactions: Single crystals of **PUM210** and **PUM210F** were dipped in DMF for 2 days to dissolve any remaining side products that may have been adhered to the crystals. Then, the crystals were soaked in a $CuCl_2$ 0.01M DMF solution at 60°C for at least three days to obtain the Cu-containing phase. During the transmetallation process the Cu-containing solution was refreshed each 24/48 hours. The occurring of the reaction could be appreciated by naked eye, since the yellow crystals of **PUM210** turned green (**Cu-PUM210**) while the white crystals of **PUM210F** turned turquois (**Cu-PUM210F**). Copper-content was determined by ICP-OES analysis.

RESULTS AND DISCUSSION

*Synthesis and Comparative Analysis of the Crystal Structures of **PUM210** and **PUM210F***. The solvothermal reaction of **bpba**, ndc and $Zn(NO_3)_2 \cdot 6H_2O$ in a 2:1:2 molar ratio in DMF at 80 °C provided **PUM210** as yellow plate crystals. The same reaction conditions were successfully applied to the synthesis of **PUM210F** but replacing **bpba** with **F-bpba**. The perfluorinated network was isolated as colourless plate crystals. The solid state structures of **PUM210** and **PUM210F** were determined by single-crystal X-ray analysis performed with synchrotron light radiation.
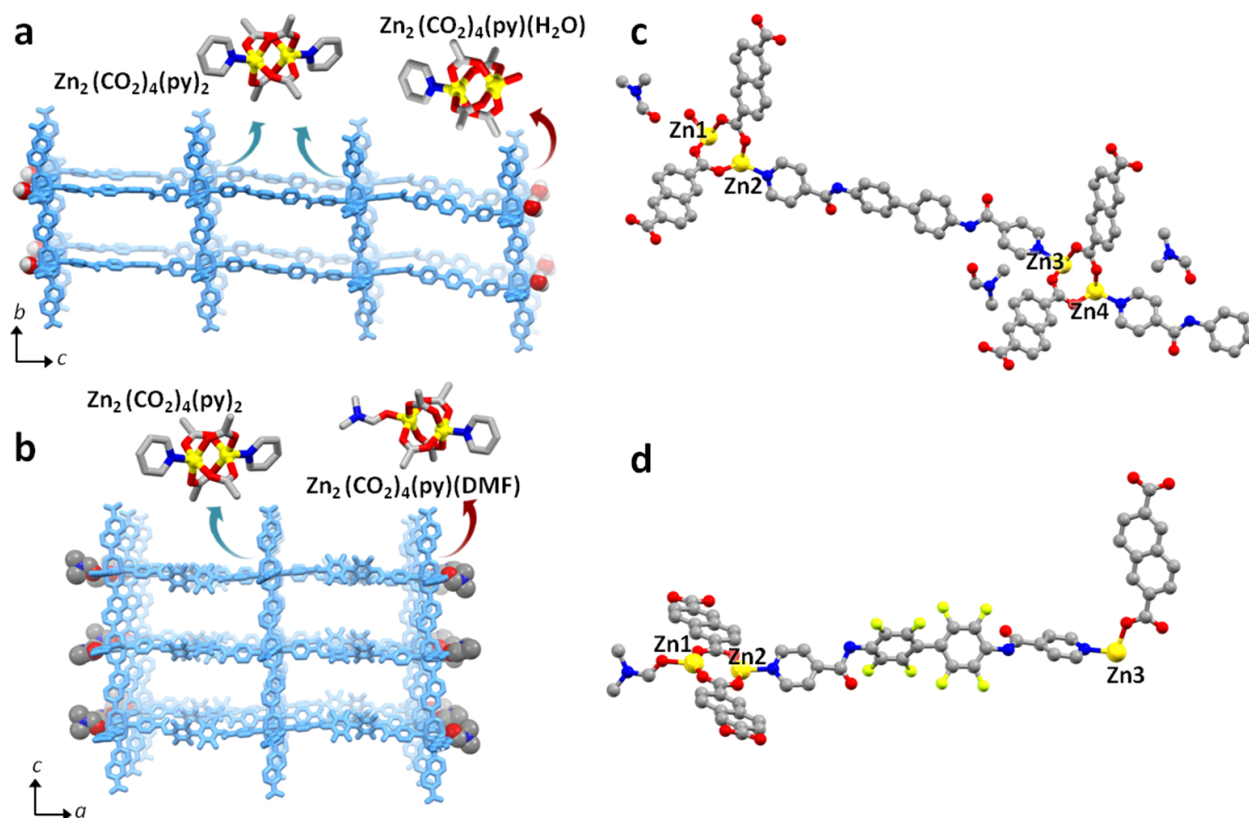
Figure 1. Framework architectures and SBUs found in **PUM210** (a) and **PUM210F** (b); (c) detail of **PUM210** (c) and **PUM210F** (d) asymmetric units.

PUM210 crystallizes in the monoclinic C2/c space group. The asymmetric unit consists of four independent Zn^{2+} cations, one and a half **bpba** ligand, four ndc^{2-} anions and three modelled DMF molecules (Figure 1c). Residual electron density (340 electrons inside each of two residual cavities of $2760Å^3$) indicates the presence of around 8 additional DMF molecules per cavity which were not possible to model. Its whole formula is then $[Zn_4(bpba)_{1.5}\cdot(ndc)_4\cdot(H_2O)]_n\cdot(DMF)_x$. The ^{1}H-NMR spectrum recorded on native crystals dissolved in a TFA-d/DMSO-d mixture indicates the presence of 4-5 molecules of DMF (see Figure S14), hence part of the included DMF was likely removed by vacuum drying prior to NMR analysis.

Notably, **PUM210** shows two different types of Zn_2 paddle-wheel SBUs.[33] Zn3 and Zn4 form the classical $[Zn_2(COO)_4(py)_2]$ unit (indicated with blue arrows in Figure 1a), where the metals lie in a square pyramidal coordination environment ensured by four bridging carboxylates and two pyridine moieties. Each SBU of this type is bridged by a **bpba** ligand oriented along *c* axis to a second type of SBU, which is a truncated paddle-wheel of the type $[Zn_2(COO)_4(py)(H_2O)]$ containing Zn1 and Zn2 (indicated with red arrow in Figure 1a). Here the truncation of the SBU is due to a molecule of water which occupies the position where a pyridine moiety was expected to be found. It is noteworthy commenting that only very few examples of truncated Zn-paddle-wheels are reported in literature.[34–36] As shown in Figure 1a, the combination of these two SBUs generates 2D sheets forming an infinite polymeric expansion along the *a* and *b* directions, which form the plane where the carboxylate square grids lie. Instead, along *c* direction, the truncation of the Zn paddle wheel leads to an interruption of the pillar motif, which is therefore limited to three **bpba** units. The coordinated water is also involved in a hydrogen bond interaction with a DMF solvent molecule (Figure 1c).

The crystallographic analysis conducted on **PUM210F** reveals that it crystallizes in the monoclinic $P2_1/c$ space group. The asymmetric unit (Figure 1d) contains three independent Zn^{2+} cations, three ndc^{2-} anions, one **F-bpba** ligand, disordered on two positions (see Supporting Info, Fig S20) and one modelled DMF molecule coordinated to Zn1 (Figure 1d). Residual electron density (1300 electrons in a void volume of $5530Å^3$) indicates the presence of around 32 additional disordered molecules of DMF in the cell. Its whole formula is then $[Zn_3(\textbf{F-bpba})_1 \cdot (ndc)_3 \cdot (DMF)]_n \cdot (DMF)_x$. ^{1}H-NMR spectroscopy conducted on native crystals digested in a TFA-d/DMSO-d mixture (see Figure S14) indicates the presence of 2.5 molecules of DMF. Again, most of the DMF molecules have likely been removed by vacuum prior to NMR analysis.

Analogously to **PUM210**, the structural motif shows again the two different Zn_2 paddle-wheel units (Figure 1c), one integral comprising Zn3 of the type $[Zn_2(COO)_4(py)_2]$, and one truncated comprising Zn1 and Zn2 of the type $[Zn_2(COO)_4(py)(DMF)]$. The different composition of the truncated SBU found in **PUM210** and **PUM210F** reflects the higher hydrophobicity expected for the perfluorinated MOF. As regard the coordination environment of the metal ions, Zn1 is bound to four carboxylic oxygens of four different ndc^{2-} anions and one oxygen belonging to a DMF molecule, whereas Zn2 is bound to four carboxylic oxygens of four different ndc^{2-} anions and one pyridine ring of a **F-bpba** ligand bridging Zn2 and Zn3. The 2D structure of the framework of **PUM210F** is then similar to the one found in **PUM210** (Figure 1b), with the two truncated SBUs being spaced only by two **F-bpba** ligands, along the crystallographic axis *a*.
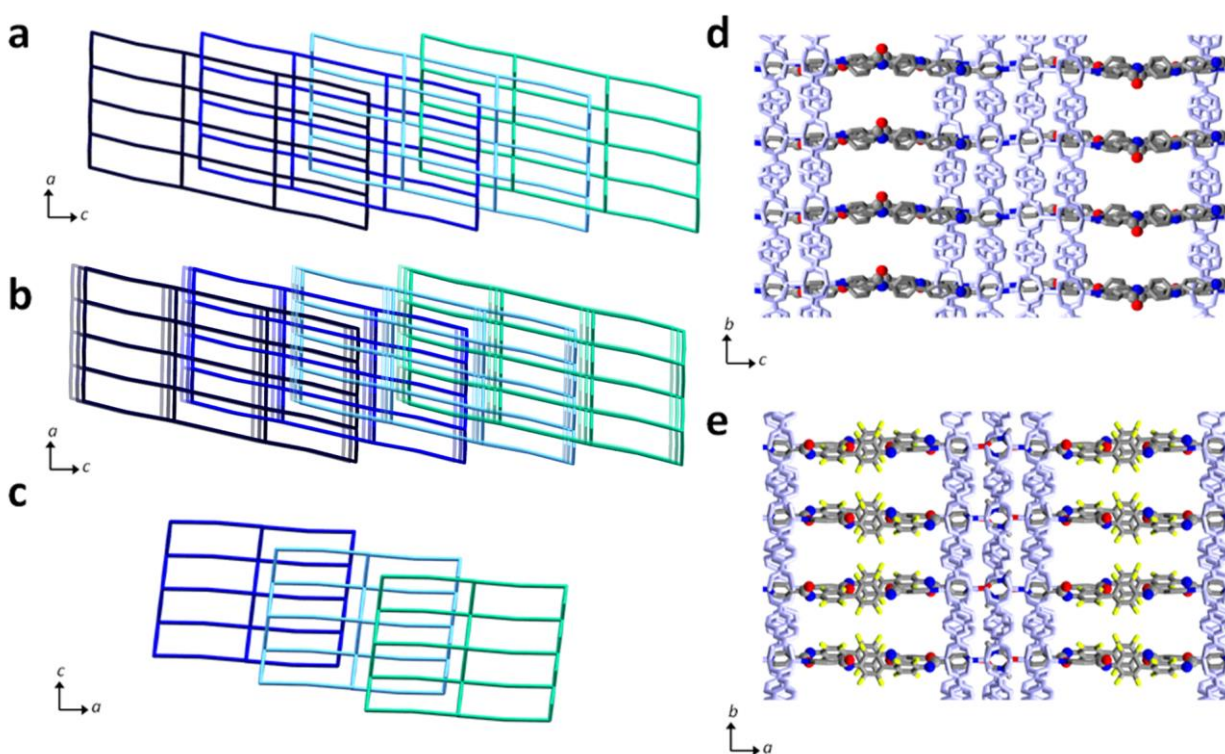
Figure 2. Simplified view of the polycatenation found in **PUM210** (a) and 1D channels along crystallographic axis a (d); (b) Interpretation of the structural disorder affecting **PUM210** arising from networks sliding along the c crystallographic direction (two additional random net positions are plotted in transparency); Simplified view of the polycatenation found in **PUM210F** (c) and 1D channels along crystallographic axis c (e).

The 3D structure of **PUM210** is generated by a triple polycatenation[37] of parallel 2D nets (Figure 2a). The resultant framework displays rectangular microporous channels running along crystallographic axis a (Figure 2d, ~7.1 x 11.5 Å^2 cross-section, determined including the van der Waals radius of atoms).[38] As shown in Figure 2d, the carboxylate planes are linked by **bpba** linkers and the channels are decorated by amide moieties of **bpba**. After removal of the solvent electron density, a unit cell void volume of 37% was calculated. A similar architecture was found in **PUM210F**, consisting of a two-fold catenated framework (Figure 2c). The lower degree of catenation should be ascribed to the higher steric hindrance of the perfluorinated biphenyl scaffold of **F-bpba**, which prevents the growth of an additional net. This allows the construction of larger channels (~8.5 x 17.2 Å^2 considering the Van der Waals radius of atoms) running along the crystallographic c axis (Figure 2e). This is also reflected in a higher fraction of void volumes, once compared with **PUM210**, which reaches 52% of the unit cell after removal of the solvent electron density and not considering the volume occupied by the disordered ligand. The different degree of polycatenation found in the two materials, appears to have a relevant impact on their structural flexibility. In fact, structural analyses show in both materials high electron density residuals close to the metal centres, situated along the paddlewheel axis, which is coincident with the direction of propagation of poly-catenation. These strong residues can be attributed to

additional positions for the SBUs and, coherently, also for the linkers. The peculiar type of disorder agrees with the presence of highly correlated diffuse scattering in the diffraction patterns (see Supporting Information, section IX) and suggests that the network is capable of moving by slight sliding of the 2D sheets one on the other, as depicted in Figure 2b for **PUM210**.

Stability. The thermal behaviour of the native MOFs was estimated by thermogravimetric analysis under nitrogen flux. TGA traces were collected using gently vacuum-dried crystals and pointed out a good thermal stability for both **PUM210** and **PUM210F**, with $T_{dec} > 340°C$ (Figure S5, Supporting Information). An initial two-step slope in the TGA trace of **PUM210** was observed in the range 25-250°C, corresponding to 23% weight loss. **PUM210F** revealed a similar behaviour with a lower weight loss, corresponding to 13%, in the same interval of temperature. The amount of thermally extruded DMF molecules agreed well with the one calculated by ^{1}H-NMR analyses performed on digested crystals (Figure S14, Supporting Information).

For applicative purposes, it is imperative that MOFs must be able to retain their 3D architecture even in the presence of moisture. For instance, the use of MOFs for post-combustion CO_2 capture, one of the most promising applications of MOFs, is limited to those which are inert towards water.[39–41] Crystals of **PUM210** quickly dull and crack once removed from DMF and stored in air for a prolonged time, as usual for carboxylate-containing Zn-based MOFs. The same is true for crystals of **PUM210F**, although degradation is significantly slower. In both cases, complete degradation occurs once the crystals are soaked in water. The robustness of the two materials towards water was properly determined by water vapour adsorption isotherms and PXRD analysis. Before being subjected to water uptake, the crystals were activated by a solvent exchange protocol using acetone and dichloromethane, followed by high vacuum at 100°C

overnight, to provide the corresponding evacuated phases (see DSC traces in Figures S10-S11). The PXRD traces of the activated phases were indicative of a substantial retention of the starting framework for **PUM210**, while significant structural modifications resulted evident in **PUM210F**. This new phase is now referred as **PUM210Fa**. The water vapour adsorption isotherms were determined plotting the water uptake against the relative humidity (p/p°) at 25°C (Figure S32), up to 1 bar of pressure. The resulting curves are sigmoidal, the water adsorption capacity at 1 bar being slightly higher for **PUM210** than for **PUM210Fa** (5.71 and 4.48 mmol/g, respectively). For the entire relative pressure interval investigated, the water uptake shown by **PUM210** is about twice the one shown by **PUM210Fa**, in agreement with the higher hydrophobicity of the latter.

Transmetallation reactions: Usually, Cu-based MOFs show higher framework stability and higher CO_2 uptake than Zn-based ones.[42–46] Our attempts to isolate the copper analogues of **PUM210** and **PUM210F** through direct synthesis proved to be ineffective. To overcome this limitation, we investigated the possibility of isolating the Cu-based MOFs through transmetalation.[3,47] This approach appeared feasible,[48] because the Zn-to-Cu substitution should be favoured according to the Irving-Williams stability series.[49] Moreover, in both frameworks there are SBUs containing terminal solvent species, water in the case of **PUM210** and DMF in the case of **PUM210F**, respectively. SBUs containing labile ligands usually lead to fast transmetallation processes.[41]
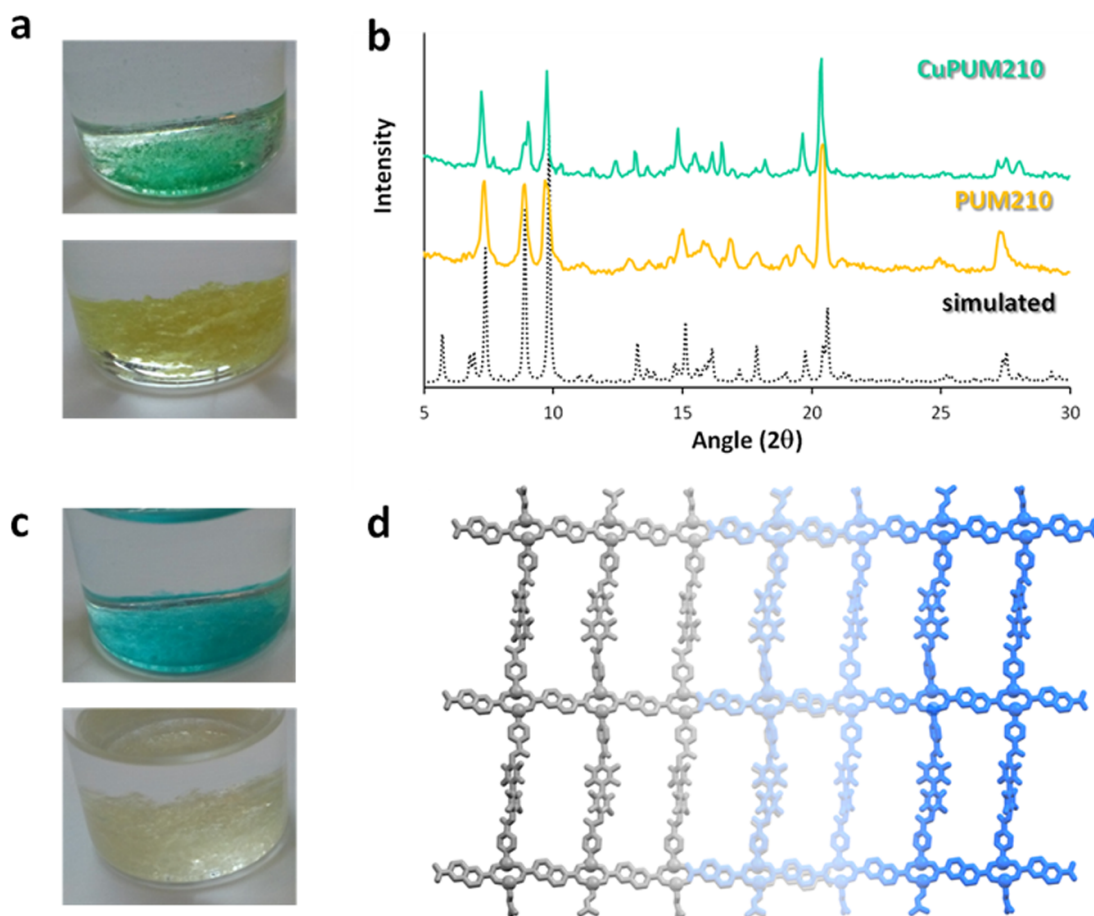
Figure 3. Chromatic variation observed during transmetallation processes of **PUM210** (a) and **PUM210F** (c); Comparison of PXRD patterns of **PUM210** (b); Superimposition of **PUM210F** (grey) and **Cu-PUM210F** (light blue) single nets, showing the retention of the framework architecture (d).

Crystals of **PUM210** and **PUM210F** were dipped into a 0.01M DMF solution of $CuCl_2$ thermostated at 60°C. After three days, in both cases the occurrence of metal-exchange was indicated by a clear color change of the crystals, as inferable from Figure 3a,c. Crystals of **PUM210** turned from yellow to green, while the crystals of **PUM210F** turned from white to turquoise. The use of $Cu(NO_3)\cdot 3H_2O$ in place of $CuCl_2\cdot 6H_2O$ led to unsatisfactory results, since the color change of the crystals was much less intense after comparable reaction times. The same

hold true carrying the reactions out at room temperature. Finally, higher copper concentrations of the transmetallating solutions or higher temperatures led to excessive fragmentation of the crystals and formation of an uncharacterized yellow side-product. Under the optimized conditions, the extent of transmetallation was established by ICP-OES (Inductively Coupled Plasma-Optical Emission Spectroscopy) analysis. After three days, in **PUM210** 28% of Zn^{2+} exchanged with Cu^{2+}, while in the case of **PUM210F** only 17% of Zn^{2+} exchanged. These new heterometallic materials are hereafter referred as **Cu-PUM210** and **Cu-PUM210F**. Single crystals of **Cu-PUM210** and **Cu-PUM210F** were subsequently picked out to be analyzed by X-ray diffraction analysis to establish the occurrence of a single-crystal-to-single-crystal (SCSC) transformation. This requires that the metal-ion exchange occurs *via* breaking and formation of metal-ligand bonds without affecting the overall MOF architecture. A close inspection of the selected crystals by optical microscopy revealed that the crystals of **Cu-PUM210F** maintained their crystal habit, whereas those of **Cu-PUM210** resulted damaged. Satisfactory X-ray diffraction was indeed observed only with the crystals of **Cu-PUM210F**. Nicely, the structural analysis revealed the retention of the starting framework, as inferable from Figure 3d, thus confirming a SCSC transformation. The asymmetric unit of **Cu-PUM210F** is then equivalent to that of the starting **PUM210F**, although in this case it was possible to model five partially occupied uncoordinated DMF molecules (see Supporting Information). The different behavior of the two types of crystals can be linked to the higher structural flexibility of the perfluorinated material conferred by the lower degree of polycatenation (double instead of triple). Noteworthy, in the F-containing framework the metal substitution had a substantial effect on the 2D networks mobility. In fact, no additional positions for the SBUs were found, thus suggesting that the polycatenated nets are now less free to slide than in the case of the starting **PUM210F**.

Prolonging the soaking to 7 days led, in the case of **PUM210**, to excessive crystals fragmentation, phenomenon not observed in the case of **PUM210F**, for which the copper content reached 32%.

Gas Adsorption Studies. To confirm the permanent porosity and check the CO_2 uptake abilities of the porous frameworks, adsorption isotherms were collected on activated MOFs. The molecular architectures described in the previous sections allow to analyse the effect deriving from different ligand functionalization (perfluorination) and post-synthetic-modifications (partial transmetallation) onto the gas-adsorption properties of the titled pillared MOFs. The materials investigated were **PUM210**, **PUM210F** and the corresponding Cu-containing materials, **Cu-PUM210** and **Cu-PUM210F**. The materials were activated following the same procedure described for the water vapour adsorption. The complete removal of the solvent molecules in the evacuated compounds was confirmed by DSC and NMR analyses (See Supporting Information). PXRD patterns evidenced structural retention passing from **Cu-PUM210** to its activated phase, as inferable from Figure 3 and Figure S17, while in the case of the perfluorinated compound, noticeable structural changes appeared (see Supporting Information). This is in agreement with the higher flexibility expected for the 210F series. Hereafter, this phase is referred as **Cu-PUM210Fa**.

The CO_2 sorption isotherms of **PUM210** and **PUM210Fa** collected at 195K exhibited a type I Langmuir behaviour,[50] indicating a favourable interaction between the amidic functionalized channels and carbon dioxide molecules during the adsorption process (Figure 4). As mentioned above, the structural modification observed after activation of **PUM210F,** decreases the cavity volume leading to a reduction of adsorbed gas and surface area in **PUM210Fa**.[51,52] The experimental BET surface area calculated by CO_2 isotherms resulted to be 491 m^2/g and 206

m^2/g for **PUM210** and **PUM210Fa**, respectively. In **PUM210** the CO_2 maximum uptake at 195K

corresponds to 27.1wt% (138.0 cm^3/g and 6.16 mmol) while, as expected, a minor percentage of

13.9wt% (71.2 cm^3/g and 3.16 mmol) was found for **PUM210Fa**. The reduced adsorptive

properties of the fluorinated networks could be assigned to a distortion of the 3D architecture

during activation with a partial pore capacity reduction.[53] CO_2 isotherm at 195K for **Cu-**

PUM210Fa (Figure 4a) showed a ~30 cm^3/g increase in CO_2 sorption capability, resulting in a

surface area of 285 m^2/g. This improvement is linked to the robustness of the MOF caused by the

presence of Cu ions, suggesting that the substitution of Zn ions with Cu ions is successful for

increasing the adsorption properties of this family of materials. Unexpectedly, the introduction of

copper does not have the same effect on **PUM210**, since the adsorptive capacity of **Cu-PUM210**

drops to 71.2 cm^3/g (Figure S31), likely due to partial degradation of the crystal framework

during the transmetallation process, as evidenced during the attempted SCSC transformation.

Under the mild conditions of 273K and 298K the CO_2 adsorption isotherms recorded up to 5 bar

of **PUM210** showed an uptake of 118.64 and 76.85 cm^3/g, respectively, whilst the **PUM210Fa**

adsorbed a minor quantity in agreement with the smaller pore capacity. The isosteric heat of

adsorption at low coverage obtained using Vant'Hoff equation is similar for both compounds: 27

kJ/mol and 28 kJ/mol for **PUM210** and **PUM210Fa**, respectively. These values exhibited good

affinity and are comparable to Zn-MOFs with a more open structure, for example Zn-MOF74.[54]
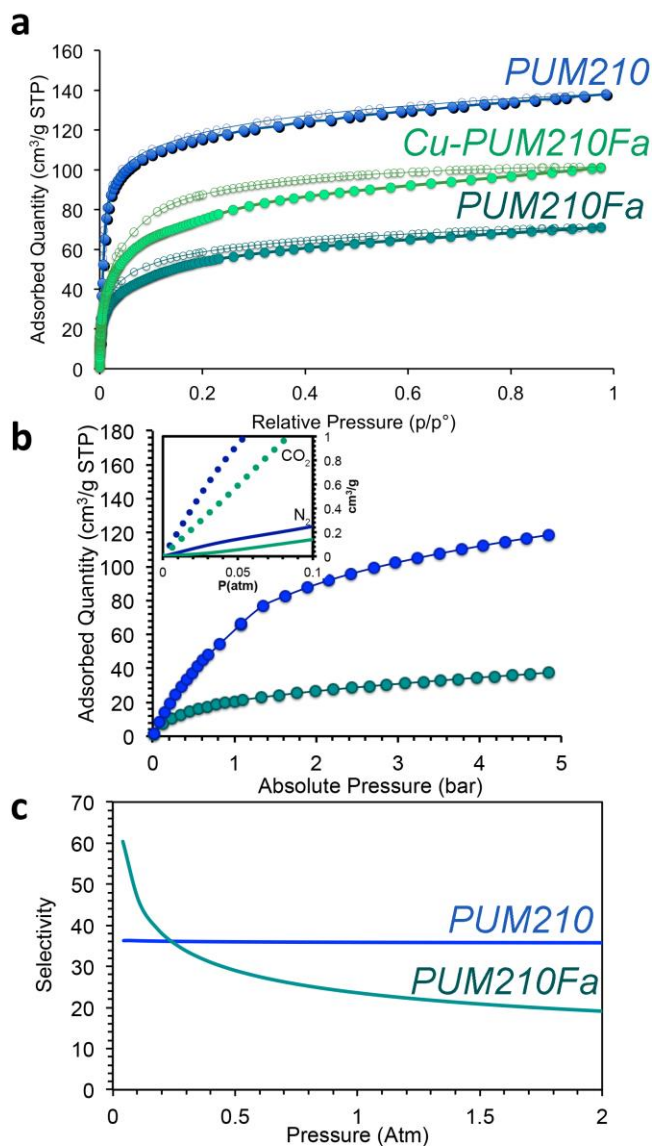
Figure 4. (a) CO_2 adsorption and desorption isotherms of **PUM210**, **PUM210Fa** and **CuPUM210Fa** performed at 195 K; (b) CO_2 adsorption isotherms collected at 273K up to 5 bar with **PUM210** (blue) and **PUM210Fa** (green), in the inset the mixture adsorption isotherms predicted IAST of **PUM210** (blue dot) and **PUM210Fa** (green line) for CO_2/N_2 (15/85); (c) Selectivity on a mixture of 15:85 of CO_2/N_2 calculated on adsorption isotherms at 273K for **PUM210** and **PUM210Fa**.

CO$_2$/N$_2$ selectivity is of importance for CO$_2$ purification from combustion emissions. For comparison, N$_2$ isotherms were collected at variable temperature on **PUM210** and **PUM210Fa**. The selectivity of CO$_2$/N$_2$ mixture (15:85) was obtained by IAST theory: at low coverage in **PUM210** at 273K the selectivity was 36 (Figure 4c) while in **PUM210Fa** the selectivity reached the value of 60 (Figure 4c). **PUM210** selectivity results to be comparable to some reported MOFs with basic functionalities in the channels, instead, **PUM210Fa** value is similar to MOFs with more polarized fluorine pendants in the structure.[55,54] To point out the sorption features of the Zn-MOFs on environmentally important guests, methane adsorption isotherms were collected at different temperatures and up to 5 bar. The isosteric heat of adsorption resulted to be 18 kJ/mol for **PUM210** and 14 kJ/mol for **PUM210Fa**, which is comparable to HKUST and MOF-5, respectively.[56]

CONCLUSIONS

Over decades, the classic disconnection approach employed in organic retrosynthesis has given a plenty of alternative routes to gain the desired substrate. More recently, MOFs projectability has attracted an active interest, as it could introduce the chance of combining functionalized linkers with tailored metallic secondary building units, by *de-novo* synthesis or through challenging PSM approaches. Herein, we have reported on the synthesis and structural characterization of novel catenated Zn^{2+}-pillared MOFs, named **PUM210** and its fluorinated analogous, **PUM210F**. The two frameworks are structurally similar, although the use of the perfluorinated linker **F-bpba** imparts peculiar features to the corresponding MOF. In fact, based on the different water adsorption isotherm profiles collected with the two MOFs, it was concluded that **PUM210F** is less hygroscopic than **PUM210**, as expected for a fluorinated MOF. Then, we have followed a transmetallation pathway in order to explore also the modification of

the metal nodes: a convenient protocol provided the heterometallic Cu^{2+}-Zn^{2+} derivatives **Cu-PUM210** and **Cu-PUM210F**. The maintenance of the parent architectures was confirmed by PXRD and, notably, by SC-XRD analysis for **Cu-PUM210** and **Cu-PUM210F**, respectively. The higher steric encumbrance of the perfluorinated biphenylene scaffold led to a lower degree of catenation, making possible the successful SCSC transformation from **PUM210F** to **Cu-PUM210F**. The activated forms of these four structurally related heteroleptic MOFs were tested for gas storage and separation. The results indicate that combination of perfluorination and transmetallation, corresponding to **Cu-PUM210F,** is a convenient strategy to reach good selectivity for CO_2 over N_2 adsorption. Current efforts are in progress in our laboratory to extend the applied combined functionalization procedure to other PUM representatives.

ASSOCIATED CONTENT

This material is available free of charge via the Internet at http://pubs.acs.org.

General Methods, NMR and IR spectra, TGA and DSC measurements, PXRD and diffuse analysis, additional gas adsorption isotherms, selectivity and isosteric heat calculation.

CCDC 1849457-1849459 contain the supplementary crystallographic data for this paper. These data can be obtained free of charge via www.ccdc.cam.ac.uk/data_request/cif, or by emailingdata_request@ccdc.cam.ac.uk, or by contacting The Cambridge Crystallographic Data Centre, 12 Union Road,Cambridge CB2 1EZ, UK; fax: +44 1223 336033.

AUTHOR INFORMATION

Corresponding Author

*paolo.pelagatti@unipr.it.

Present Addresses

⊥ current affiliation: Department of Chemical Engineering, Delft University of Technology, Van

der Maasweg 9, 2629 HZ, Delft, The Netherlands.

Author Contributions

The manuscript was written through contributions of all authors.

REFERENCES

(1) Slater, A. G.; Cooper, A. I. Function-Led Design of New Porous Materials. *Science* **2015**, *348* (6238), aaa8075.

(2) Moreau, F.; Kolokolov, D. I.; Stepanov, A. G.; Easun, T. L.; Dailly, A.; Lewis, W.; Blake, A. J.; Nowell, H.; Lennox, M. J.; Besley, E.; et al. Tailoring Porosity and Rotational Dynamics in a Series of Octacarboxylate Metal-Organic Frameworks. *Proc. Natl. Acad. Sci.* **2017**, *114* (12), 3056–3061.

(3) Lalonde, M.; Bury, W.; Karagiaridi, O.; Brown, Z.; Hupp, J. T.; Farha, O. K. Transmetalation Routes to Metal Exchange within Metal–organic Frameworks. *J. Mater. Chem. A* **2013**, *1* (18), 5453–5468.

(4) Wang, Z.; Cohen, S. M. Postsynthetic Modification of Metal–organic Frameworks. *Chem. Soc. Rev.* **2009**, *38* (5), 1315.

(5) Tanabe, K. K.; Cohen, S. M. Postsynthetic Modification of Metal–organic Frameworks -A Progress Report. *Chem. Soc. Rev.* **2011**, *40* (2), 498–519.

(6) Deria, P.; Mondloch, J. E.; Karagiaridi, O.; Bury, W.; Hupp, J. T.; Farha, O. K. Beyond

Post-Synthesis Modification: Evolution of Metal–organic Frameworks via Building Block Replacement. *Chem. Soc. Rev.* **2014**, *43* (16), 5896–5912.

(7)   Xu, Y.; Vermeulen, N. A.; Liu, Y.; Hupp, J. T.; Farha, O. K. SALE-Ing a MOF-Based "Ship of Theseus." Sequential Building-Block Replacement for Complete Reformulation of a Pillared-Paddlewheel Metal-Organic Framework. *Eur. J. Inorg. Chem.* **2016**, *2016* (27), 4345–4348.

(8)   Li, B.; Wen, H.-M.; Zhou, W.; Chen, B. Porous Metal − Organic Frameworks for Gas Storage and Separation: What, How, and Why? *J. Phys. Chem. C* **2014**, *5*, 3468−3479.

(9)   Schoedel, A.; Ji, Z.; Yaghi, O. M. The Role of Metal–Organic Frameworks in a Carbon-Neutral Energy Cycle. *Nat. Energy* **2016**, *1* (4), 16034.

(10)   Yu, J.; Xie, L.-H.; Li, J.-R.; Ma, Y.; Seminario, J. M.; Balbuena, P. B. CO_2 Capture and Separations Using MOFs: Computational and Experimental Studies. *Chem. Rev.* **2017**, *117* (14), pp 9674–9754.

(11)   Keskin, S.; van Heest, T. M.; Sholl, D. S. Can Metal-Organic Framework Materials Play a Useful Role in Large-Scale Carbon Dioxide Separations? *ChemSusChem* **2010**, *3* (8), 879–891.

(12)   Trickett, C. A.; Helal, A.; Al-Maythalony, B. A.; Yamani, Z. H.; Cordova, K. E.; Yaghi, O. M. The Chemistry of Metal–organic Frameworks for CO_2 Capture, Regeneration and Conversion. *Nat. Rev. Mater.* **2017**, *2* (8), 17045.

(13)   Bhattacharya, B.; Ghoshal, D. Selective Carbon Dioxide Adsorption by Mixed-Ligand Porous Coordination Polymers. *CrystEngComm* **2015**, *17* (44), 8388–8413.

(14)   Vaidhyanathan, R.; Iremonger, S. S.; Shimizu, G. K. H.; Boyd, P. G.; Alavi, S.; Woo, T. K. Direct Observation and Quantification of CO_2 Binding within an Amine-Functionalized Nanoporous Solid. *Science* **2010**, *330* (6004), 650–653.

(15)   Zhang, L.; Jiang, K.; Li, Y.; Zhao, D.; Yang, Y.; Cui, Y.; Chen, B.; Qian, G. Microporous Metal–Organic Framework with Exposed Amino Functional Group for High Acetylene Storage and Excellent C_2H_2 /CO_2 and C_2H_2 /CH_4 Separations. *Cryst. Growth Des.* **2017**, *17* (5), 2319–2322.

(16)   Chen, D. M.; Xu, N.; Qiu, X. H.; Cheng, P. Functionalization of Metal-Organic Framework via Mixed-Ligand Strategy for Selective CO_2 Sorption at Ambient Conditions. *Cryst. Growth Des.* **2015**, *15* (2), 961–965.

(17)   Lee, C.; Huang, H.; Liu, Y.; Luo, T.; Lee, G.; Peng, S.; Jiang, J.; Chao, I.; Lu, K. Cooperative Effect of Unsheltered Amide Groups on CO_2 Adsorption Inside Open-Ended Channels of a Zinc(II) − Organic Framework,. *Inorg. Chem.* **2013**, *52* (7)*, 3*962–3968. (18)   Safarifard, V.; Rodríguez-Hermida, S.; Guillerm, V.; Imaz, I.; Bigdeli, M.; Tehrani, A. A.; Juanhuix, J.; Morsali, A.; Casco, M. E.; Silvestre-Albero, J.; et al. Influence of the Amide Groups in the CO2/N2 Selectivity of a Series of Isoreticular,

Interpenetrated Metal-Organic Frameworks. *Cryst. Growth Des.* **2016**, *16* (10), 6016–6023.

(19) Alsmail, N. H.; Suyetin, M.; Yan, Y.; Cabot, R.; Krap, C. P.; Lü, J.; Easun, T. L.; Bichoutskaia, E.; Lewis, W.; Blake, A. J.; et al. Analysis of High and Selective Uptake of CO_2 in an Oxamide-Containing {$Cu_2(OOCR)_4$}-Based Metal-Organic Framework. *Chem. - A Eur. J.* **2014**, *20* (24), 7317–7324.

(20) Zheng, B.; Bai, J.; Duan, J.; Wojtas, L.; Zaworotko, M. J. Enhanced CO_2 Binding Affinity of a High-Uptake Rht-Type Metal-Organic Framework Decorated with Acylamide Groups. *J. Am. Chem. Soc.* **2011**, *133* (4), 748–751.

(21) Bent, H. A. Structural Chemistry of Donor-Acceptor Interactions. *Chem. Rev.* **1968**, *68* (5), 587–648.

(22) Zhang, D.-S.; Chang, Z.; Li, Y.-F.; Jiang, Z.-Y.; Xuan, Z.-H.; Zhang, Y.-H.; Li, J.-R.; Chen, Q.; Hu, T.-L.; Bu, X.-H. Fluorous Metal-Organic Frameworks with Enhanced Stability and High H_2/CO_2 Storage Capacities. *Sci. Rep.* **2013**, *3* (1), 3312.

(23) Chen, T.-H.; Popov, I.; Zenasni, O.; Daugulis, O.; Miljanić, O. Š. Superhydrophobic Perfluorinated Metal–organic Frameworks. *Chem. Commun.* **2013**, *49* (61), 6846.

(24) Chen, C. X.; Wei, Z. W.; Qiu, Q. F.; Fan, Y. Z.; Cao, C. C.; Wang, H. P.; Jiang, J. J.; Fenske, D.; Su, C. Y. A Porous Zn(II)-Metal-Organic Framework Constructed from Fluorinated Ligands for Gas Adsorption. *Cryst. Growth Des.* **2017**, *17* (4), 1476–1479.

(25) Pachfule, P.; Das, R.; Poddar, P.; Banerjee, R. Structural, Magnetic, and Gas Adsorption Study of a Series of Partially Fluorinated Metal-Organic Frameworks (HF-MOFs). *Inorg. Chem.* **2011**, *50* (Scheme 1), 3855–3865.

(26) Luo, X.; Yin, Z.; Zeng, M.; Kurmoo, M. The Construction, Structures, and Functions of Pillared Layer Metal-Organic Frameworks. *Inorg. Chem. Front.* **2016**, *3*, 1208–1226.

(27) Huang, S. L.; Lin, Y. J.; Li, Z. H.; Jin, G. X. Self-Assembly of Molecular Borromean Rings from Bimetallic Coordination Rectangles. *Angew. Chemie - Int. Ed.* **2014**, *53* (42), 11218–11222.

(28) Davide Balestri, Davide Costa, Alessia Bacchi, Lucia Carlucci, P. P. Linker Dependent Dimensionality in Zn(II)-Coordination Polymers Containing a Flexible Bis-Pyridyl-Bis-Amide Ligand. *Polyhedron*-submitted

(29) Balestri, D.; Bacchi, A.; Scilabra, P.; Pelagatti, P. Extension of the Pd-Catalyzed CN Bond Forming Reaction to the Synthesis of Large Polydentate Ligands Containing NH Functions. *Inorganica Chim. Acta* **2017**, *470*, 416-422.

(30) Lausi, A.; Polentarutti, M.; Onesti, S.; Plaisier, J.R.; Busetto, E.; Bais, G.; Barba, L.; Cassetta, A.; Campi, G.; Lamba, D. Status of the Crystallography Beamline at Elettra. *Eur. Phys. J. Plus* **2015**, *130*, 1–8.

(31)   Sheldrick, G. M. A Short History of SHELX. *Acta Crystallogr. Sect. A Found. Crystallogr.* **2007**, *64* (1), 112–122.

(32)   Dolomanov, O. V.; Bourhis, L. J.; Gildea, R. J.; Howard, J. A. K.; Puschmann, H. OLEX2: A Complete Structure Solution, Refinement and Analysis Program. *J. Appl. Crystallogr.* **2009**, *42* (2), 339–341.

(33)   Köberl, M.; Cokoja, M.; Herrmann, W. A.; Kühn, F. E. From Molecules to Materials: Molecular Paddle-Wheel Synthons of Macromolecules, Cage Compounds and Metal-Organic Frameworks. *Dalt. Trans.* **2011**, *40* (26), 6834–6859.

(34)   Wang, S.; Xiong, S.; Wang, Z.; Du, J. Rational Design of Zinc-Organic Coordination Polymers Directed by N-Donor Co-Ligands. *Chem. - A Eur. J.* **2011**, *17* (31), 8630–8642.

(35)   Chun, H.; Jung, H.; Seo, J. Isoreticular Metal-Organic Polyhedral Networks Based on 5-Connecting Paddlewheel Motifs. *Inorg. Chem.* **2009**, *48* (5), 2043–2047.

(36)   Chun, H. Low-Level Self-Assembly of Open Framework Based on Three Different Polyhedra: Metal-Organic Analogue of Face-Centered Cubic Dodecaboride. *J. Am. Chem. Soc.* **2008**, *130* (3), 800–801.

(37)   Carlucci, L.; Ciani, G.; Proserpio, D. M. Polycatenation, Polythreading and Polyknotting in Coordination Network Chemistry. *Coord. Chem. Rev.* **2003**, *246* (1–2), 247–289.

(38)   Batsanov, S. S. Van Der Waals Radii of Elements. *Inorg. Mater. Transl. from Neorg. Mater. Orig. Russ. Text* **2001**, *37* (9), 871–885.

(39)   Furukawa, H.; Ga, F.; Hudson, M. R.; Yaghi, O. M. Water Adsorption in Porous Metal − Organic Frameworks and Related Materials. *J. Am. Chem. Soc.* **2014,** *136*(11), 4369-4381

(40)   Wang, C.; Liu, X.; Keser Demir, N.; Chen, J. P.; Li, K. Applications of Water Stable Metal–organic Frameworks. *Chem. Soc. Rev.* **2016**, *45* (18), 5107–5134.

(41)   Canivet, J.; Fateeva, A.; Guo, Y.; Coasne, B.; Farrusseng, D. Water Adsorption in MOFs: Fundamentals and Applications. *Chem. Soc. Rev.* **2014**, *43* (16), 5594–5617.

(42)   Song, X.; Jeong, S.; Kim, D.; Lah, M. S. Transmetalations in Two Metal–organic Frameworks with Different Framework Flexibilities: Kinetics and Core–shell Heterostructure. *CrystEngComm* **2012**, *14* (18), 5753.

(43)   Pal, T. K.; De, D.; Neogi, S.; Pachfule, P.; Senthilkumar, S.; Xu, Q.; Bharadwaj, P. K. Significant Gas Adsorption and Catalytic Performance by a Robust CuII-MOF Derived through Single-Crystal to Single-Crystal Transmetalation of a Thermally Less-Stable ZnII-MOF. *Chem. - A Eur. J.* **2015**, *21* (52), 19064–19070.

(44)   Xiao, Z.; Wang, Y.; Zhang, S.; Fan, W.; Xin, X.; Pan, X.; Zhang, L.; Sun, D. Stepwise Synthesis of Diverse Isomer MOFs via Metal-Ion Metathesis in a Controlled Single-Crystal-to-Single-Crystal Transformation *Cryst. Growth Des.* **2017**, *17* (8), 4084–4089.

(45) Yang, J.; Wang, X.; Dai, F.; Zhang, L.; Wang, R.; Sun, D. Improving the Porosity and Catalytic Capacity of a Zinc Paddlewheel Metal-Organic Framework (MOF) through Metal-Ion Metathesis in a Single-Crystal-to-Single-Crystal Fashion. *Inorg. Chem.* **2014**, *53* (19), 10649–10653.

(46) Pal, T. K.; De, D.; Senthilkumar, S.; Neogi, S.; Bharadwaj, P. K. A Partially Fluorinated, Water-Stable Cu(II)-MOF Derived via Transmetalation: Significant Gas Adsorption with High CO2 Selectivity and Catalysis of Biginelli Reactions. *Inorg. Chem.* **2016**, *55* (16), 7835–7842.

(47) Brozek, C. K.; Dincă, M. Cation Exchange at the Secondary Building Units of Metal-Organic Frameworks. *Chem. Soc. Rev.* **2014**, *43*, 5456–5467.

(48) Pal, T. K.; Neogi, S.; Bharadwaj, P. K. Versatile Tailoring of Paddle-Wheel ZnII Metal-Organic Frameworks through Single-Crystal-to-Single-Crystal Transformations. *Chem. - A Eur. J.* **2015**, *21* (45), 16083–16090.

(49) Deria, P.; Mondloch, J. E.; Karagiaridi, O.; Bury, W.; Hupp, J. T.; Farha, O. K. Beyond Post-Synthesis Modification: Evolution of Metal–organic Frameworks via Building Block Replacement. *Chem. Soc. Rev. Chem. Soc. Rev* **2014**, *5896* (43), 5896–5912.

(50) Brunauer, S.; Deming, L. S.; Deming, W. E.; Teller, E. On a Theory of the van Der Waals Adsorption of Gases. *J. Am. Chem. Soc.* **1940**, *62* (7), 1723–1732.

(51) Chang, G.; Wen, H.; Li, B.; Zhou, W.; Wang, H.; Alfooty, K.; Bao, Z.; Chen, B. A Fluorinated Metal-Organic Framework for High Methane Storage at Room Temperature. *Cryst. Growth Des.* **2016**, *16* (6), 3395–3399.

(52) Chang, ganggang; Li, B.; Wang, H.; Bao, Z.; Yildirim, T.; Yao, Z.-Z.; Xiang, S.; Zhou, W.; Chen, B. A Microporous Metal–organic Framework with Polarized Trifluoromethyl Groups for High Methane Storage. *Chem. Commun.* **2015**, *51*, 14789–14792.

(53) Bureekaew, S.; Sato, H.; Matsuda, R.; Kubota, Y.; Hirose, R.; Kim, J.; Kato, K.; Takata, M.; Kitagawa, S. Control of Interpenetration for Tuning Structural Flexibility Influences Sorption Properties. *Angew. Chemie - Int. Ed.* **2010**, *49* (42), 7660–7664.

(54) Queen, W. L.; Hudson, M. R.; Bloch, E. D.; Mason, J. A.; Gonzalez, M. I.; Lee, J. S.; Gygi, D.; Howe, J. D.; Lee, K.; Darwish, T. A.; et al. Comprehensive Study of Carbon Dioxide Adsorption in the Metal–organic Frameworks M $_2$ (Dobdc) (M = Mg, Mn, Fe, Co, Ni, Cu, Zn). *Chem. Sci.* **2014**, *5* (12), 4569–4581.

(55) Zhang, Z.; Yao, Z.-Z.; Xiang, S.; Chen, B. Perspective of Microporous Metal–organic Frameworks for CO $_2$ Capture and Separation. *Energy Environ. Sci.* **2014**, *7* (9), 2868.

(56) Mason, J. A.; Veenstra, M.; Long, J. R. Evaluating Metal–organic Frameworks for Natural Gas Storage. *Chem. Sci.* **2014**, *5* (1), 32–51.

SYNOPSIS The structural and gas-sorption effects deriving from ligand perfluoruration and partial transmetallation have been evaluated for a series of structurally related pillared MOFs

FOR TABLE OF CONTENTS ONLY